

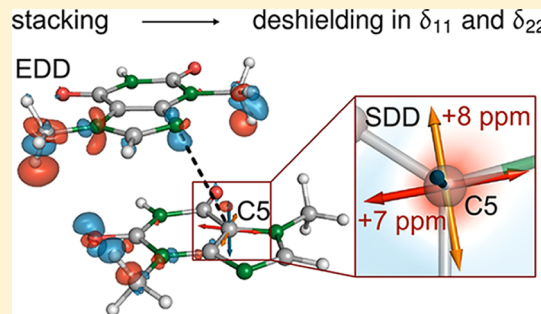
Intermolecular Interactions in Crystalline Theobromine as Reflected in Electron Deformation Density and ^{13}C NMR Chemical Shift Tensors

Kateřina Bouzková,[†] Martin Babinský,^{†,‡} Lucie Novosadová,[†] and Radek Marek^{*,†,‡,§}

[†]CEITEC—Central European Institute of Technology, [‡]National Center for Biomolecular Research, and [§]Department of Chemistry, Masaryk University, Kamenice 5/A4, CZ-62500 Brno, Czech Republic

Supporting Information

ABSTRACT: An understanding of the role of intermolecular interactions in crystal formation is essential to control the generation of diverse crystalline forms which is an important concern for pharmaceutical industry. Very recently, we reported a new approach to interpret the relationships between intermolecular hydrogen bonding, redistribution of electron density in the system, and NMR chemical shifts (Babinský et al. *J. Phys. Chem. A*, 2013, 117, 497). Here, we employ this approach to characterize a full set of crystal interactions in a sample of anhydrous theobromine as reflected in ^{13}C NMR chemical shift tensors (CSTs). The important intermolecular contacts are identified by comparing the DFT-calculated NMR CSTs for an isolated theobromine molecule and for clusters composed of several molecules as selected from the available X-ray diffraction data. Furthermore, electron deformation density (EDD) and shielding deformation density (SDD) in the proximity of the nuclei involved in the proposed interactions are calculated and visualized. In addition to the recently reported observations for hydrogen bonding, we focus here particularly on the stacking interactions. Although the principal relations between the EDD and CST for hydrogen bonding (HB) and stacking interactions are similar, the real-space consequences are rather different. Whereas the C–H···X hydrogen bonding influences predominantly and significantly the in-plane principal component of the ^{13}C CST perpendicular to the HB path and the C=O···H hydrogen bonding modulates both in-plane components of the carbonyl ^{13}C CST, the stacking modulates the out-of-plane electron density resulting in weak deshielding (2–8 ppm) of both in-plane principal components of the CST and weak shielding (~ 5 ppm) of the out-of-plane component. The hydrogen-bonding and stacking interactions may add to or subtract from one another to produce total values observed experimentally. On the example of theobromine, we demonstrate the power of this approach to identify and classify the intermolecular forces that govern the packing motifs in crystals and modulate the NMR CSTs.



1. INTRODUCTION

Molecules in crystalline organic, pharmaceutical, and biological compounds are held together by intermolecular forces that are traditionally classified, for example, as strong and weak hydrogen bonds and C–H··· π and π ··· π interactions. Depending on the conditions of crystallization, a compound may develop into various crystal forms that are characterized by different networks of intermolecular contacts.^{1,2} These forms, known as polymorphs, may notably differ in their physical and pharmaceutical properties.³ Therefore, structural characterization of the individual forms based on description of the most important intermolecular contacts became important for controlling the generation of polymorphs.⁴

For a detailed description of the molecular and supramolecular structure of crystalline materials, solid-state NMR spectroscopy represents a very efficient and powerful tool.⁵ Its multinuclear capability enables to probe the electronic environment of various nuclei in the molecule and to give us a picture of the present intramolecular and intermolecular interactions. From the NMR measurables, chemical shifts have been successfully used in the study of local molecular structure⁶

and packing arrangements in crystals.⁷ In many cases, isotropic chemical shifts act as a “fingerprint” for identification of polymorphs. Even more sensitive to crystal effects than isotropic shifts are chemical shift tensors (CSTs).⁸ It has been shown in many cases that an effect observed in the isotropic shift is due to a change in only one of the three tensor components, and as such, the effect is three times as large in this component. In other cases, there is almost no difference observed in the isotropic shift, but there are significant effects on the individual components that compensate each other, with some of them shifting to larger chemical shift values and others to smaller chemical shift values. Both the principal values and orientation of the CST with respect to the molecular frame are sensitive to the electron density distribution around the nucleus of interest and reflect the local molecular structure and intermolecular interactions.^{9,10} Although the ^{15}N nucleus is more sensitive to local structure, the ^{13}C CSTs are studied very

Received: March 15, 2013

frequently, mainly because they are more easily determined at natural abundance.

In the study of the relationship between the NMR chemical shifts and the structure, quantum chemical calculations of magnetic shielding have long been used.¹¹ Nuclear magnetic shielding is a response property that can be defined quantum mechanically and directly calculated. Later it can be converted to chemical shift by subtracting the shielding constant of the nucleus of interest from the shielding constant of an appropriate reference compound. Calculations further provide the orientation of the CST in the molecular frame, which cannot be directly determined from the experimental measurements on powder samples. Currently, the dominant approach to the calculation of magnetic shielding for medium size and large molecules is based on the density functional theory (DFT).¹²

There are different methods available to computationally describe how the crystal packing influences CSTs. They can be classified into those that use the electrostatic models,¹³ the cluster models,^{14,15} and periodic boundary conditions.¹⁶ In electrostatic models, the crystal packing is simulated by a finite charge distribution and, as such, fail to reproduce the experimental data when the crystal environment is dominated by other effects than electrostatic interactions. Cluster models represent the packing by a finite number of neighboring molecules. This approach can be computationally demanding, but allows for a study of individual intermolecular effects by repeating the calculation for various supramolecular arrangements. On the contrary, the methods that use periodic boundary conditions include automatically all possible intermolecular effects by exploiting the translation symmetry inherent in crystals, and as such, they are much less computationally demanding than the cluster methods.

In our recent work,¹⁷ we demonstrated how the cluster model can be used for identification of intermolecular contacts that govern the packing motifs in crystals. For this purpose, we compared the calculated CSTs for a single molecule and for several clusters that were selected according to the X-ray diffraction data. The modulation of the CST originates in changes in the distribution of the electron density around the nucleus in question. We calculated the differences in the electron density distribution between the isolated molecule and the clusters and visualized them as the electron deformation density (EDD) patterns.¹⁷ Shortly, the EDD patterns show regions of the molecule and of its closest surroundings where the electron density increases or decreases^{18,19} due to formation of intermolecular contacts. The EDD patterns can be correlated with the changes in the CSTs of the nuclei involved in the interactions. For better understanding of this relationship, the changes in the isotropic magnetic shielding (shielding deformation density, SDD) in the proximity of the nucleus in question can also be calculated and visualized in the real space.¹⁷

Here, we use this approach to describe the ¹³C CSTs and their relation to the crystal packing for theobromine (Figure 1), a well-known purine-based heart stimulant. The full set of experimentally determined and calculated ¹³C CSTs for theobromine are reported here and discussed for the first time. The sensitivity of the ¹³C CSTs of the purine ring to intermolecular interactions was described previously.²⁰ This study aims at showing how the connection between CSTs and the crystal structure, particularly crystal stacking, of biologically important compounds can be monitored and analyzed.

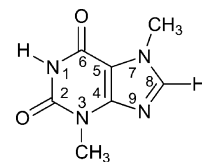


Figure 1. Structure and atom numbering of theobromine.

2. EXPERIMENTAL AND THEORETICAL METHODS

2.1. Sample. Theobromine (Figure 1) was purchased from Sigma-Aldrich and used without further purification. Identity of the structure of the sample with the structure deposited in the Cambridge Structural Database (CSD)²¹ was confirmed by using X-ray powder diffraction.

2.2. Solid-State NMR Spectroscopy. Solid-state NMR experiments were performed at room temperature on a Bruker AVANCE-500 spectrometer operating at frequencies 500.13 MHz (¹H) and 125.77 MHz (¹³C). A Bruker 4 mm MAS probe was used for all the measurements. The ¹³C chemical shifts were referenced to crystalline α -glycine as a secondary reference ($\delta_{st} = 176.03$ ppm for carbonyl carbon). ¹³C CP/MAS spectra were recorded with 4 ms contact time and a recycle delay of 30 s. The ramped amplitude (RAMP) shape pulse was used during the cross-polarization and two-pulse phase-modulated (TPPM) decoupling during the acquisition. Spectral assignments were done with the use of nonquaternary suppression (NQS)²² and cross-polarization phase inversion (CPPI)²³ pulse sequences and from the comparison with the calculated values. Program DMFIT²⁴ was used to obtain principal components of the ¹³C CSTs from the MAS sideband patterns. Throughout this program, the Haeberlen-Mehring convention for description of the chemical shift tensor is used. Following this convention, three parameters of the chemical shift tensor can be determined from the MAS sideband pattern: δ_{iso} , the isotropic value, is the average value of the principal components and corresponds to the center of gravity of the line shape; CSA = $\delta_{zz} - \delta_{iso}$, the anisotropy, describes the largest separation from the center of gravity; and $\delta = (\delta_{yy} - \delta_{xx})/(\delta_{zz} - \delta_{iso})$, the asymmetry, indicates by how much the line shape deviates from that of an axially symmetric tensor. δ_{iso} can be determined from the centerband position and the two other parameters from an analysis of sideband intensities.²⁵ From the definition of these three parameters for the principal components of the chemical shift tensor follows $\delta_{zz} = \text{CSA} + \delta_{iso}$, $\delta_{yy} = \delta_{iso} - \text{CSA}(1 - \eta)/2$, $\delta_{xx} = \delta_{iso} - \text{CSA}(1 + \eta)/2$. The principal components obtained from the DMFIT program were subsequently ordered according to the IUPAC rules:²⁶ $\delta_{11} \geq \delta_{22} \geq \delta_{33}$.

2.3. Calculation of NMR Chemical Shifts. The geometry of the C, N, and O atoms as determined by X-ray diffraction²¹ was fixed and the positions of the protons were optimized within the Gaussian 09.A2 code.²⁷ Then, the nuclear magnetic shieldings were calculated. All of the calculations were performed by using DFT. The three-parameter hybrid functional of Becke B3LYP^{28–30} was used with the 6-31G*³¹ basis set to optimize the positions of protons. Additionally, the M06³² hybrid functional of Truhlar and Zhao was tested with the same basis set. The components of the shielding tensors were computed by the gauge-including atomic orbital (GIAO) method. The 6-311G**³³ basis set was employed for the calculations using the B3LYP functional or the hybrid functional of Perdew, Burke, and Ernzerhof PBE0.³⁴ Results

Table 1. DFT Calculated^a Isotropic Chemical Shifts and Principal Components of the ¹³C CSTs^b for Selected Clusters of Theobromine, the Experimental Chemical Shifts, and Root-Mean-Square Deviations (RMSDs) between the Calculated and Experimental Values (ppm)

atom		M1	HB2	HB3	HB4	HB7	S7	HBS13	expt.
C2	δ_{iso}	148.5	150.2	150.9	150.9	151.1	149.4	151.2	153.1
C4	δ_{iso}	149.1	148.0	149.0	148.8	148.7	149.7	149.4	150.0
C5	δ_{iso}	103.5	104.3	104.5	104.5	105.0	107.2	108.2	108.1
C6	δ_{iso}	149.7	149.8	151.0	151.0	150.9	151.5	152.3	154.9
C8	δ_{iso}	138.8	138.4	139.3	142.3	143.7	138.6	143.0	142.6
RMSD (δ_{iso})		4.1	3.8	3.0	2.6	2.6	2.9	1.5	
C2	δ_{11}	235	222	224	223	219	236	220	223
	δ_{22}	113	130	130	131	136	119	140	140
	δ_{33}	98	98	98	98	99	93	94	96
RMSD (CST-C2)		17.1	5.9	5.9	5.3	3.7	14.4	2.1	
C4	δ_{11}	211	209	211	211	211	213	213	217
	δ_{22}	164	162	163	161	160	167	163	161
	δ_{33}	73	73	73	74	76	69	72	72
RMSD (CST-C4)		3.9	4.7	3.7	3.7	4.2	4.5	2.6	
C5	δ_{11}	140	142	140	138	138	147	145	151
	δ_{22}	125	127	128	129	130	133	136	131
	δ_{33}	46	45	46	46	47	42	43	42
RMSD (CST-C5)		7.6	5.9	7.0	7.9	8.1	2.6	4.5	
C6	δ_{11}	243	241	237	237	237	247	239	240
	δ_{22}	120	121	129	129	127	127	135	138
	δ_{33}	86	87	87	87	88	81	83	87
RMSD (CST-C6)		10.6	9.8	5.5	5.5	6.6	8.3	2.9	
C8	δ_{11}	207	206	207	206	206	209	208	208
	δ_{22}	130	130	132	148	151	134	152	148
	δ_{33}	80	79	79	73	74	74	69	71
RMSD (CST-C8)		11.6	11.4	10.3	1.6	2.7	8.3	2.6	
RMSD (CST-All)		11.1	8.0	6.8	5.2	5.4	8.6	3.1	

^aGeometry of C, N, and O atoms for anhydrous theobromine determined by X-ray diffraction²¹ was fixed and positions of protons for the individual clusters were optimized by using B3LYP/6-31G* method. Nuclear shieldings were calculated by B3LYP/6-311G**. Subsequently, chemical shifts were calculated using following equation: $\delta_i = \sigma_{\text{st}} - \sigma_i + \delta_{\text{st}}$. The shielding of α -glycine cluster ($\sigma_{\text{C-13}}$ of the C=O group; $\sigma_{\text{st}} = 0.5$ ppm) was calculated by the same method as used for theobromine, and the experimental chemical shift $\delta_{\text{st}} = 176.03$ ppm for carbonyl carbon in glycine was employed. ^bBoldface numbers highlight significant intermolecular effects.

obtained for the four combinations of functionals were virtually identical; the largest differences in the calculated shieldings were 3 ppm (Table S1 in the Supporting Information). Subsequently, the chemical shifts were calculated using the following equation: $\delta_i = \sigma_{\text{st}} - \sigma_i + \delta_{\text{st}}$. The α -glycine cluster²⁰ was built, and its shielding was calculated by the same methods ($\sigma_{\text{C-13}}$ of the C=O group: $\sigma_{\text{st}} = 0.5$ ppm). The experimental chemical shift $\delta_{\text{st}} = 176.03$ ppm for the carbonyl carbon in glycine was employed. Finally, the RMSDs between the theoretical and experimental data were calculated.

2.4. Calculations of EDD, SDD, and Interaction Energies. The Gaussian 09.A2 suite of programs was also employed for the calculations of the electron deformation density (EDD) and the shielding deformation density (SDD). The B3LYP functional and the 6-311G** basis set were used. Because of quite modest size of the basis set, the counterpoise correction by Boys and Bernardi³⁵ was used during the calculations involving only parts of molecular clusters.

Single-point interaction energy calculations were performed using the TURBOMOLE 6.03³⁶ suite at the SCS-MP2³⁷ level of theory and employing Dunning's aug-cc-pVTZ^{38,39} basis set. The counterpoise correction was used also in this case. Resolution of identity (RI)⁴⁰ approximation was employed in order to speed up the calculations, and all orbitals with energies lower than -3.0 hartree were kept frozen.

3. RESULTS AND DISCUSSION

3.1. General Considerations. The basic framework topology of theobromine (Figure 1) was obtained from the Cambridge Structural Database (CSD).²¹ The identity of the structure with the sample used for the NMR study was confirmed by using X-ray powder diffraction. For the determination of the isotropic chemical shifts and the principal components of the ¹³C CSTs of the purine ring of theobromine, one-dimensional CP/MAS experiment was used. Assignment of the isotropic chemical shifts was carried out using the NQS and CPPI editing techniques and by comparison with the calculated data. For the analysis of the MAS sideband pattern, DMFIT program was used (see Section 2.2). To minimize the error arising from the analysis and to estimate the standard deviation, the CST parameters were determined at several MAS rates and the obtained principal components were averaged. The values of the individual MAS rates, the average values, and the standard deviations can be found in the Supporting Information (Table S2). The average values that are discussed in the text are summarized in Table 1.

To understand the effect of crystal packing on the ¹³C NMR CSTs, we determined them also theoretically by using density functional theory (DFT). We calculated the CSTs for a single theobromine molecule and then for several supramolecular clusters.

The clusters were chosen according to the X-ray diffraction data that are available in CSD.²¹ The asymmetric unit in the crystal structure of theobromine contains two molecules. However, their crystal environment differs only slightly and only one set of signals is observed in the NMR spectrum (Figure 2), with slight broadening of C2 signal. Therefore, only

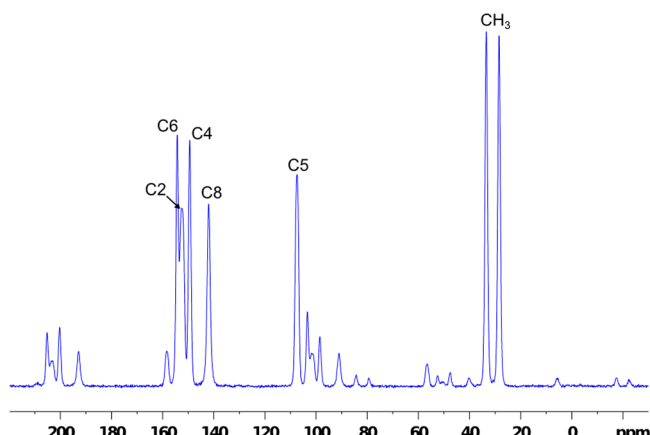


Figure 2. ^{13}C CP/MAS spectrum of theobromine acquired at 6.4 kHz. The isotropic shifts of individual carbon atoms are labeled.

one of the two molecules was considered as the central molecule of the cluster, which enabled us to use smaller clusters for the inspection of the relevant intermolecular interactions and hence speed up the calculation. The validity of this approach was confirmed by calculating the NMR CSTs twice for the cluster **HB10**—once for each of the two molecules—with the differences being less than 1 ppm for the isotropic shifts and no more than 2 ppm for the principal components (Table S3 in the Supporting Information). The heavy-atom coordinates for these calculations were taken from the X-ray diffraction data and the positions of protons were optimized individually (see Section 2.3). We also tried to optimize the geometry of the whole central molecule of the cluster (i.e. including the heavy atoms), but it influenced the results only marginally; the differences in the calculated principal components of the CSTs did not exceed 4 ppm (Table S1 in the Supporting Information).

The NMR CSTs are always calculated for the central molecule of the cluster. The clusters were chosen so that the effect of a particular intermolecular contact can be followed and are designated according to the number of molecules that they contain and according to the type of cluster—**HB** clusters contain only in-plane molecules and are selected to examine hydrogen bonding (*vide infra*), the **S** cluster contains only molecules above and under the plane of the central molecule and reveals the effect of stacking, and the **HBS** cluster contains both the types to simulate a total crystal environment of the central molecule. Hence, in our case, the methods using periodic boundary conditions^{16,41} to describe the effect of crystal packing as a whole^{42–44} were not suitable. Cartesian coordinates of all the clusters are given in the Supporting Information.

Comparison of the calculated ^{13}C NMR CSTs with the experimental data is provided in Table 1. The experimental values in the last column are compared with the values calculated for an isolated molecule (**M1**) and for the supramolecular clusters. The orientations of the principal

components of the ^{13}C CSTs for the largest cluster of theobromine (**HBS13** in Table 1) are depicted in Figure 3.

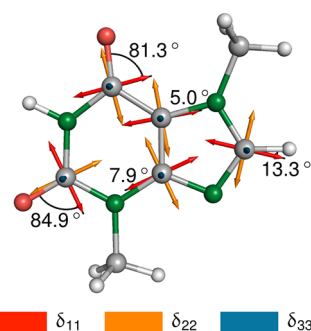


Figure 3. Orientations of the ^{13}C NMR CSTs for aromatic carbons in theobromine calculated for cluster HBS13.

For all of the atoms of the purine ring, the δ_{11} and δ_{22} components lie within the plane of the purine ring, and the δ_{33} component is oriented perpendicular to the plane. The angles that the δ_{11} components assume with the selected bonds are also given. For the smaller clusters and the isolated molecule, the angles change less than 8° with the only exception being carbon C5 where the difference between **M1** and **HBS13** is 13.3° (the angle $\delta_{11} - \text{C5}-\text{N7}$ in **M1** is 18.3°).

In Table 1, the differences between the experimental and the calculated NMR CSTs for the individual clusters are characterized by root-mean-square deviations. Significant differences in individual shifts that can be attributed to a certain intermolecular contact are given in bold. As anticipated, the effect of hydrogen bonding in the crystal is clearly visible for the carbonyl carbons C2 and C6 and for the protonated carbon C8. In addition, C6 together with C5 seem to be considerably influenced by the stacking of molecules in the crystal.

As the changes in NMR chemical shifts are related to the changes in distribution of electron density around the nucleus in question, we were interested in comparing the CSTs with the EDD patterns calculated for the same clusters. The process of calculating the EDD was described in our previous paper.¹⁷ The resulting patterns provide us with a pictorial form of changes of the electron density in real space induced by the intermolecular contacts. The EDD pattern calculated for the cluster **HB7** is shown in Figure 4 as an example. Blue regions in this figure represent an increase of electron density and red regions indicate the decrease of electron density as a result of intermolecular contacts formed between the central molecule and the surrounding molecules in the cluster.

In addition, we use the plots of isotropic shielding deformation density (SDD).¹⁷ They are based on calculation of isotropic magnetic shielding on a grid around molecule.^{45,46} Similarly to the EDD patterns, the blue regions in these patterns represent increased isotropic shielding (and hence decreased NMR chemical shift for atomic nucleus) and red regions indicate decreased shielding (increased chemical shift). Comparing the EDD and the SDD patterns indicates how the changes in electron density influence isotropic magnetic shielding around the nucleus in question.

In some cases, we qualitatively estimated the strength of an intermolecular contact also by calculating single-point interaction energies for dimers featuring the interaction.

The methodology is first demonstrated on the effects of hydrogen bond $\text{C2}=\text{O}\cdots\text{H}-\text{N}$, weak interaction $\text{C2}=$

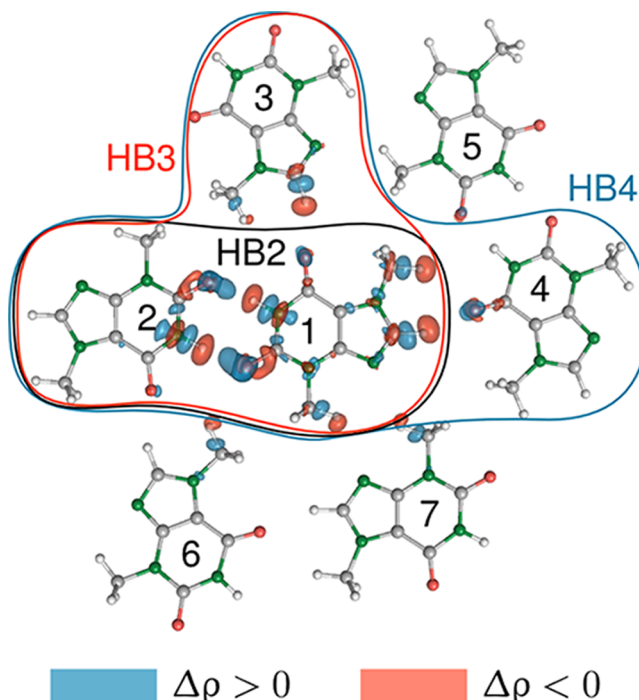


Figure 4. Visualization of the EDD for a hydrogen-bonded cluster **HB7** of theobromine. Numbering of the molecules corresponds to the composition of the smaller clusters.

O···H₃C—N, and stacking interactions on the ¹³C NMR CST of C2, and subsequently, we discuss the other carbon atoms of theobromine.

3.2. Carbon C2. If we compare the experimentally determined CST of carbon C2 with the values calculated for an isolated molecule (**M1** in Table 1), we observe significant differences mainly in two in-plane principal components ($\Delta\delta_{11} = 12$, $\Delta\delta_{22} = 27$, $\Delta\delta_{33} = 2$). It is a clear indication that there are crystal forces which modulate the chemical shift of C2.

Hydrogen Bonding. To examine the effect of hydrogen bonds, we calculated the EDD pattern for an in-plane cluster that contains six molecules around the central molecule (**HB7**, Figure 4). The strongest interaction is observed between the two molecules that are found in the asymmetric unit of the crystal structure (molecules 1 and 2 in Figure 4, cluster **HB2**). As found from the X-ray diffraction data, the two molecules form two hydrogen bonds: N1—H···O'—C' and C2=O···H'—N'. Interaction energy for this dimer was calculated to be -11.5 kcal mol⁻¹ (i.e., -5.8 kcal mol⁻¹ per bond). If we have a closer look at the EDD pattern in the C2=O···H—N region (Figure 5a and 5b), we may clearly identify a polarization of the C=O bond due to the presence of the hydrogen bond—the electron density is accumulated at the oxygen atom (major blue area) and decreases at the atom C2 (predominant red area in π space). The decreased electron density around C2 should result in increase in the chemical shift. Indeed, if we compare the calculated $\delta_{iso}(C2)$ for **M1** and **HB2**, it increases from 148.5 ppm to 150.2 ppm. To explain the changes in the principal components of the CST, we have to go step further and have a look at how the changes in the electron density distribution influence magnetic shielding. For this purpose, we calculated the SDD pattern for the **HB2** cluster. The SDD pattern is shown in Figure 6a. According to the figure, the magnetic shielding decreases in the direction of the C=O bond (red area) and increases in an area approximately

perpendicular to this bond (blue area). We further see that the $\delta_{22}(C2)$ NMR CST component lies approximately in the area of the red lobe, while the $\delta_{11}(C2)$ passes the area of the blue lobe. As a result, the NMR chemical shift should increase in the $\delta_{22}(C2)$ CST component, while in the $\delta_{11}(C2)$ a decrease should be observed. This is in excellent agreement with the calculated NMR CST for the **HB2** cluster; when compared with the values for **M1**, the $\delta_{11}(C2)$ decreases from 235 ppm to 222 ppm, while for the $\delta_{22}(C2)$ the effect is reverse: it increases from 113 to 130 ppm (Table 1, $\Delta\delta_{22} = +17$ ppm in Figure 6a).

Weak Hydrogen Bonding. The CST components calculated for the cluster **HB2** are much closer to the experimentally determined values than the components obtained for the isolated molecule. Nevertheless, we wanted to know whether there is any additional effect that influences the CST of carbon C2 and could further improve the agreement between the experiment and calculation.

In Figure 4, another molecule that is close to the carbon C2 of the central molecule is molecule 6. The red lobe on the methyl proton of molecule 6 indicates the polarization of the C—H bond and formation of a weak hydrogen bond with the oxygen of the central molecule. This contact should have the same effect on the C2=O group of the central molecule as the C2=O···H—N hydrogen bond, but significantly smaller. Hence, for the cluster containing molecules 1 and 6, the $\delta_{22}(C2)$ CST component should further increase and the $\delta_{11}(C2)$ component should slightly decrease. In the calculated CST for this cluster, it is indeed observed—when compared with the values for **HB2**, there is a 4 ppm increase ($\Delta\delta_{22} = +4$ ppm in Figure 6b) in $\delta_{22}(C2)$ and 3 ppm decrease in $\delta_{11}(C2)$. Also, the EDD and the SDD patterns for this interaction look very similar to those obtained for **HB2** but are much less pronounced (compare a and c in Figure 5 and a and b in Figure 6). Furthermore, the interaction energy for this pair of molecules was calculated to be -3.2 kcal mol⁻¹, which is approximately a half of what was estimated for one conventional hydrogen bond in **HB2** (-5.8 kcal mol⁻¹).

Stacking Interactions. The CST components, calculated for the cluster **HB7** that includes the conventional as well as the weak hydrogen bond, agree with the experimentally determined magnitudes quite well. However, some effect of stacking on the CST of carbon C2 can also be observed. To examine the effect of stacking, we calculated the CSTs for a cluster that contains three molecules above and three molecules below the central molecule (**S7** in Table 1). The stacking interactions induce moderate deshielding of $\delta_{22}(C2)$ by +6 ppm ($\Delta\delta_{22} = +6$ ppm in Figure 6c) whereas $\delta_{11}(C2)$ is almost unaffected. This modulation is probably induced by the interaction of the carbonyl oxygen with atoms of neighboring layers. Further, the modulation of $\delta_{33}(C2)$ by -5 ppm (see Table 2) is probably induced by the direct interaction of C2 with C8' from neighboring crystal layer (see also the discussion of C8). The EDD and SDD patterns for stacking interactions are visualized in Figure 5 (e and f) and Figure 6c.

Total Effect. For the largest cluster **HBS13** (see Figures 5g, 5h and 6d), which is a combination of clusters **HB7** and **S7** and includes hydrogen bonding ($\Delta\delta_{11} = -13$, $\Delta\delta_{22} = +17$), weak hydrogen bonding ($\Delta\delta_{11} = -3$, $\Delta\delta_{22} = +4$), and stacking interactions ($\Delta\delta_{11} = +1$, $\Delta\delta_{22} = +6$), all these effects sum up ($\Delta\delta_{11} = -15$, $\Delta\delta_{22} = +27$) to produce data with excellent agreement with experimental NMR chemical shifts (see Table 1).

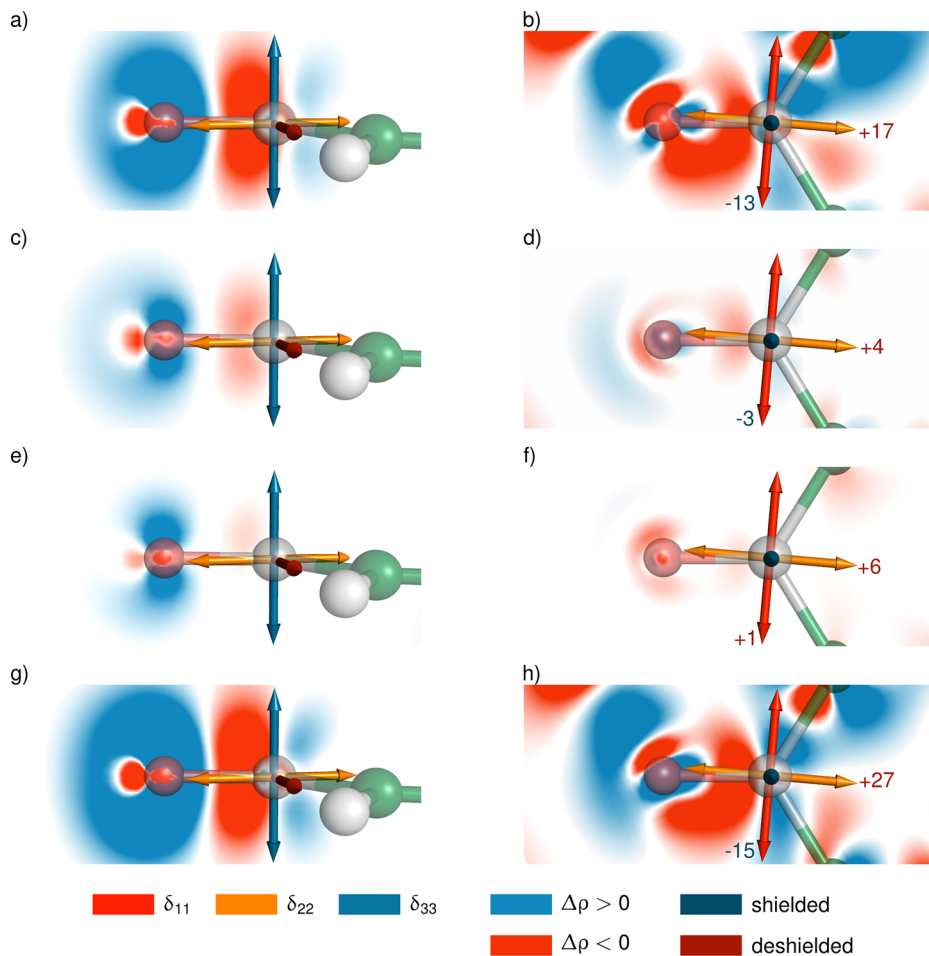


Figure 5. Visualization of the out-of-plane ($\delta_{22}|\delta_{33}$, left) and in-plane ($\delta_{11}|\delta_{22}$, right) slices of the EDD for atom C2 in theobromine. (a and b) HB2. (c and d) Cluster composed of molecules 1 and 6 (weak hydrogen bonding, see Figure 4). (e and f) S7. (g and h): HBS13. The arrows schematically represent the calculated relative orientations of the in-plane principal components of the ^{13}C CST, and the numbers denote the calculated changes in the magnitude of these components upon formation of the clusters.

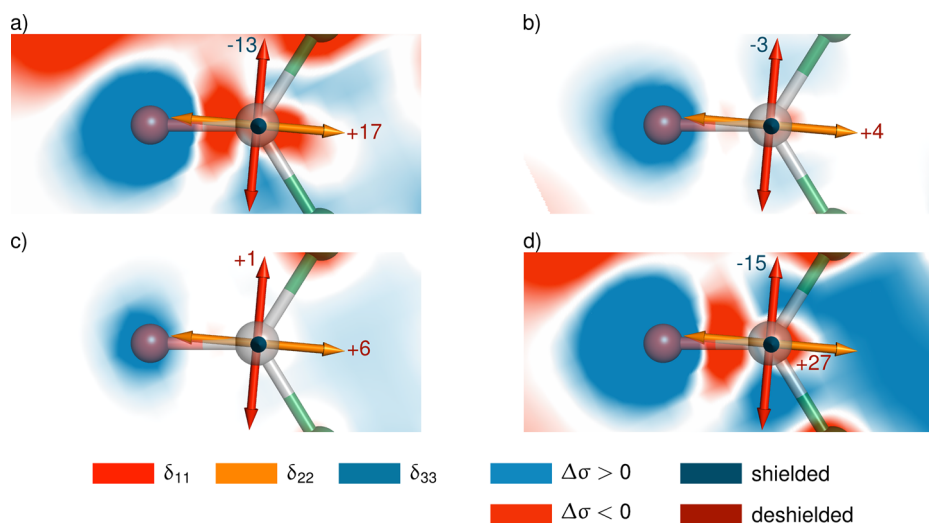


Figure 6. Visualization of the in-plane ($\delta_{11}|\delta_{22}$) slices of the SDD for atom C2 in theobromine. (a) HB2. (b) Cluster composed of molecules 1 and 6 (see Figure 4). (c) S7. (d) HBS13. The arrows schematically represent the calculated relative orientations of the in-plane principal components of the ^{13}C NMR CST, and the numbers denote the calculated changes in the magnitude of these components upon formation of the clusters.

3.3. Carbons C4 and C5. The quaternary bridgehead carbons of the purine ring do not form any hydrogen bonds and their CSTs are also rather insensitive to hydrogen bonds

formed by neighboring atoms.²⁰ This fact is confirmed in our study of theobromine, where the CSTs of the quaternary carbons C4 and C5 calculated for an isolated molecule **M1** are

Table 2. Differences in ^{13}C NMR CSTs (in ppm) Calculated between Various Clusters (HB7, S7, HBS13) and Monomer^a

		C2	C4	C5	C6	C8
HB7	δ_{11}	-17	0	-2	-6	-1
	δ_{22}	+23	-4	+5	+9	+21
	δ_{33}	0	+3	+1	0	-6
S7	δ_{11}	+1	+2	+7	+4	+2
	δ_{22}	+6	+3	+8	+7	+4
	δ_{33}	-5	-4	-4	-5	-6
HBS13	δ_{11}	-15	+2	+5	-4	+1
	δ_{22}	+27	-1	+11	+15	+22
	δ_{33}	-4	-1	-3	-3	-11

^aFor Cartesian coordinates, see the Supporting Information.

almost the same as those calculated for the largest HB cluster **HB7** (Table 1).

The CST calculated for atom C4 is in good agreement with the experimentally determined values, and no significant improvement of the result was observed for the largest cluster **HBS13**, which includes also the stacking effects. Although one may identify a weak modulation of component $\delta_{22}(\text{C4})$ and $\delta_{33}(\text{C4})$ by hydrogen bonding of neighboring atoms in **HB7** ($\Delta\delta_{22} = -4$ ppm, $\Delta\delta_{33} = +3$ ppm), these effects are almost perfectly compensated for by those induced by stacking in **S7** ($\Delta\delta_{22} = +3$ ppm, $\Delta\delta_{33} = -4$ ppm) resulting in marginal total changes for **HBS13** as compared with **M1** (see Table 2).

For atom C5, the δ_{11} CST component calculated for the HB clusters is significantly smaller than the experimental one, which could indicate some effect of stacking. Indeed, in the stacked cluster **S7** an increase is observed in the δ_{11} CST component and the agreement with the experiment improves. From the examination of the EDD pattern calculated for the whole cluster **S7** we found that one of the molecules in the upper layer is most likely responsible for the effect (Figure 7).

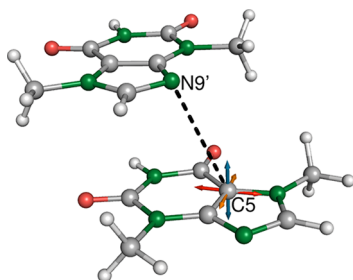


Figure 7. Stacking interaction between these two molecules is most likely responsible for the change in the CST of carbon C5.

The main interaction that is responsible for this modulation is that between π system of the C5 carbon and N9' atom of the neighboring stacked molecule (Figure 7 and Figure S1 (Supporting Information)). We observe a decrease of electron density in the proximity of carbon C5 above the ring plane (red lobe in Figure 8a), which is in agreement with an increase in its isotropic NMR chemical shift. To confirm this relationship and to further analyze the contact, we calculated the SDD pattern for these two molecules (for an in-plane slice, see Figure 8b). A deshielding area around C5 induced by stacking between these two molecules is situated in the plane of the purine ring (Figure 8b). If we compare the CST values calculated for the monomer **M1** or HB clusters (e.g., **HB7**) and those calculated for the cluster **S7** (Table 1), an increase is indeed found in both the in-

plane CST components δ_{11} (+7 ppm) and δ_{22} (+8 ppm). This deshielding effect originates probably in more effective $\sigma_{\text{C}-\text{C}} \rightarrow \pi^*$ and $\sigma_{\text{C}-\text{N}} \rightarrow \pi^*$ transitions. Whereas the effects of hydrogen bonding and stacking compensate each other to some extent for δ_{11} (-2 and +7 ppm) and δ_{33} (+1 and -4 ppm), these two effects operate in the same direction for δ_{22} (+5 and +8 ppm) resulting in 11 ppm difference between **M1** and **HBS13** (see Table 2). We can conclude that the interaction between the layers of molecules in the crystal packing of theobromine is the interaction that has quite important effect on the CST of the quaternary carbon C5.

3.4. Carbon C6. Atom C6 is another carbonyl carbon in the structure of theobromine. In contrast to C2, the difference between the experimentally determined CST of this carbon and the values calculated for an isolated molecule is observed mainly in the δ_{22} principal component and is significantly smaller. It seems, therefore, that the CST of this carbon is influenced by weaker intermolecular contacts than the CST of C2.

Hydrogen Bonding. Hydrogen bonds with the molecule 2, which strongly influence the CST of C2, have negligible effect on the CST of C6, as documented by the values calculated for the cluster **HB2** (Table 1). Another molecule close to atom C6 of the central molecule is molecule 3 (as numbered in Figure 4). According to the EDD pattern calculated for the two-molecule cluster including this molecule (molecules 1 and 3 from Figure 4), a weak hydrogen bond $\text{C}_6=\text{O} \cdots \text{H}-\text{C}$ is formed between the central molecule and the C8-H group of the neighboring molecule. The EDD pattern induced by this interaction is very similar to that for the conventional hydrogen bond $\text{C}_2=\text{O} \cdots \text{H}-\text{N}$, but the deformations are smaller (Figures 9a and 10a), which indicates that the interaction is weaker.

To confirm the difference in the strength of the intermolecular interaction, we have calculated the interaction energies (IEs) for the cluster **HB2** and for the two-molecule cluster composed of the molecules 1 and 3. For the latter pair containing only the weak $\text{C}=\text{O} \cdots \text{H}-\text{C}$ hydrogen bonds (C_8-H and $-\text{CH}_3$) the calculated IE is $-4.2 \text{ kcal mol}^{-1}$ ($\Delta\delta_{11} = -6$ ppm, $\Delta\delta_{22} = +9$ ppm), and for the pair of the cluster **HB2**, which is connected by two conventional $\text{C}=\text{O} \cdots \text{H}-\text{N}$ hydrogen bonds, the IE value is $-11.5 \text{ kcal mol}^{-1}$ ($\Delta\delta_{11} = -17$ ppm, $\Delta\delta_{22} = +23$ ppm). These numbers support the EDD model and confirm that the different changes in the calculated CST for atoms C2 and C6 are due to the formation of intermolecular interactions of different strengths.

The EDD pattern for atom C6 is dominated by a red lobe (decrease of the electron density) in the π subspace of this carbon that should result in an increase in the isotropic chemical shift. Molecule 3 is included in all the HB clusters that are larger than **HB2**. It is reflected in $\delta_{\text{iso}}(\text{C6})$, which is slightly larger in these clusters. As clear from Table 2, the difference is due to decrease in the δ_{11} (-6 ppm) and increase in the δ_{22} (+9 ppm) CST components. These changes are reflected in the SDD pattern calculated for the pair of molecules 1 and 3 (Figures 9b and 10b). The red area corresponding to a decrease of magnetic shielding is found approximately along the $\text{C}=\text{O}$ bond, which is the direction of the $\delta_{22}(\text{C6})$ CST component, whereas the blue region is found in the direction of the $\delta_{11}(\text{C6})$ component. The CST components calculated for the cluster **HB3** and for the larger HB clusters are nearly the same, which indicates that the weak hydrogen bond $\text{C}_6=\text{O} \cdots \text{H}-\text{C}$ with the molecule 3 is the only important intermolecular interaction

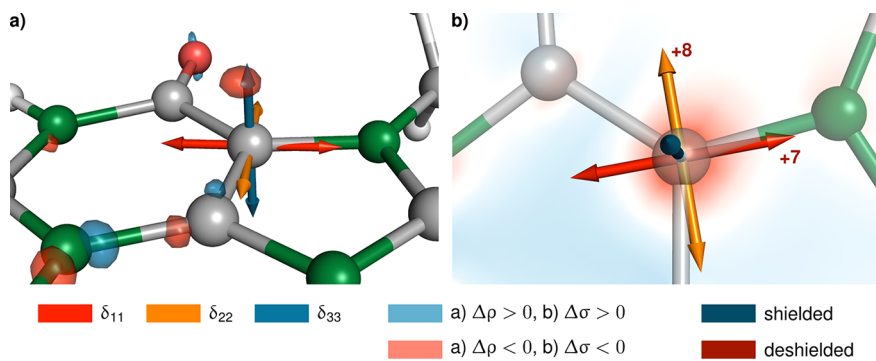


Figure 8. Visualization of the EDD (a) and in-plane slice of the SDD (b) for the two-molecule cluster of theobromine from Figure 7. The arrows schematically represent the calculated relative orientations of the principal components of the ^{13}C CST of carbon C5.

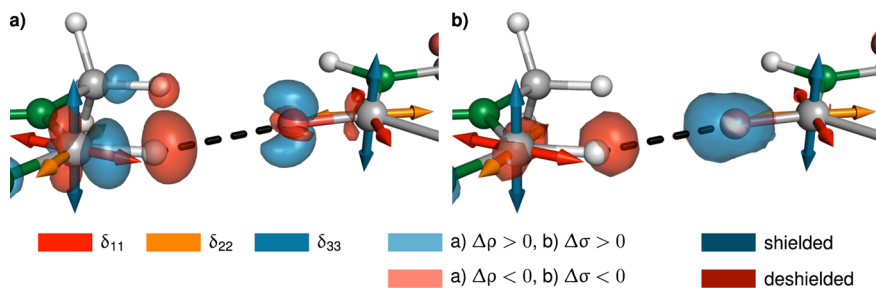


Figure 9. Visualization of the EDD (a) and the SDD (b) for the two-molecule cluster composed of molecules 1 (right) and 3 (left)—see Figure 4 for the global arrangement. The arrows schematically represent the calculated relative orientations of the principal components of the ^{13}C CSTs of carbons C8 (C—H) and C6 (C=O).

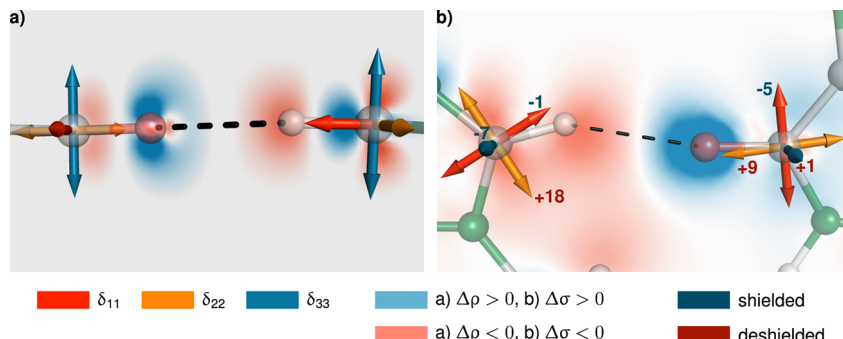


Figure 10. Visualization of the out-of-plane slice of the EDD (a) and in-plane slice of the SDD (b) for atoms C8 (C—H) and C6 (C=O) in theobromine. The arrows schematically represent the calculated relative orientations of the principal components of the ^{13}C CSTs, and the numbers denote the calculated changes in the magnitude of these components upon formation of the two-molecule cluster composed of molecules 1 and 3 (see Figure 4).

in the plane of the central molecule which influences the CST of atom C6.

Stacking Interactions. The $\delta_{22}(\text{C}6)$ CST component calculated for the largest HB cluster is closer to the experimentally determined value than the one obtained for an isolated molecule. However, there is still a considerable deviation, which indicates the missing effect of stacking interactions.

If we compare the CST of carbon C6 calculated for M1 with the values obtained for S7 (see Table 2), we observe an increase in two in-plane components of the CST ($\Delta\delta_{11} = +4$ ppm, $\Delta\delta_{22} = +7$ ppm) and decrease in the out-of-plane component ($\Delta\delta_{33} = -5$ ppm). While HB and S effects on the $\delta_{11}(\text{C}6)$ largely compensate each other, the effect of these two interactions sum up to the difference of +15 ppm for $\delta_{22}(\text{C}6)$ in HBS13. The EDD and SDD patterns around the atom C6 in

the cluster S7 are similar to those described for C5 and are shown in Figures S2 and S3 (Supporting Information).

The CST values calculated for the cluster HBS13, which is a combination of clusters HB7 and S7, show that the stacking interaction is comparably important for the modulation of the CST of carbon C6 as the weak hydrogen bond C6=O \cdots H—C (see Table 2).

3.5. Carbon C8. CSTs of protonated carbons of the purine ring are known for their sensitivity to the formation of weak hydrogen bonds, which is predominantly manifested in the δ_{22} component. In the structure of theobromine, the only protonated carbon of the purine ring is carbon C8. If we compare its experimentally determined CST with the values calculated for an isolated molecule (M1 in Table 1), the largest difference is indeed observed in the δ_{22} component (see Table 2).

As found from the EDD pattern calculated for the cluster **HB7**, a weak hydrogen bond C8—H···O=C is formed between the central molecule and the molecule 4 (Figure 4). Significance of this interaction for the CST of carbon C8 is clear from Table 1—the magnitudes of the CST components are not influenced by the presence of the molecules 2 and 3 (clusters **HB2** and **HB3**, respectively), but when molecule 4 is added (**HB4**), a 16 ppm increase in the $\delta_{22}(\text{C8})$ component is observed. The CST components calculated for the cluster **HB4** do not change significantly for the larger clusters that include the molecule 4. Hence, it can be concluded that the weak hydrogen bond C8—H···O=C with the molecule 4 is the most important HB interaction influencing the CST of carbon C8.

A detail of the EDD pattern for the region of the C8—H···O=C hydrogen bond (Figure 9a and Figure 10a) shows that the electron density decreases in the area of the hydrogen and the π space of the carbon atom (red lobes) and is accumulated in the σ subspace of carbon atom (blue lobe). An increase in electron density in the σ space and its decrease in the π part (see Figure 10a) could enhance the $\sigma_{\text{C}-\text{H}} \rightarrow \pi^*$ transitions responsible for the deshielding effect, as described recently.¹⁷ Further, we calculated the SDD pattern for the system of molecules 1 and 4. At the carbon C8, the pattern is dominated by a red lobe that indicates decrease of the shielding mainly in the direction perpendicular to the HB and is oriented in the same way like the $\delta_{22}(\text{C8})$ CST component (Figures 9b and 10b). Hence, it is not surprising that the increase in the $\delta_{\text{iso}}(\text{C8})$ is due to increase in the δ_{22} component, as confirmed by the values calculated for the isolated molecule **M1** and for the cluster **HB7** (Table 2). This HB interaction induced also a weak shielding of the out-of-plane component (see Table 2, $\Delta\delta_{33} = -6$ ppm). The $\pi \cdots \pi$ stacking, particularly the interaction of C8 with carbon C2' of the neighboring layer, induces another shielding of this component of the CST ($\Delta\delta_{33} = -6$ ppm). The shielding contributions of the HB and S interactions to $\Delta\delta_{33}(\text{C8})$ are comparable in their magnitudes and result in the total effect of -11 ppm in **HBS13**.

4. CONCLUSIONS

We demonstrated how the combination of the ^{13}C NMR CSTs and the EDD patterns, both calculated for reasonably selected clusters, can be used for detecting the presence and characterizing the strength of intermolecular interactions in crystals.

By using this approach, we characterized the effect of crystal packing on the ^{13}C NMR CSTs of theobromine. We found that there are two conventional hydrogen bonds that influence the CST of carbon C2, which is a carbonyl carbon with the oxygen participating in the interaction; we found three weak hydrogen bonds that influence the CSTs of carbons C2, C6, and C8. With the help of the SDD patterns, we determined how the presence of these interactions is recoded in magnetic shielding in the real-space around the molecule and interpreted the differences in chemical shifts calculated for an isolated molecule and those which were determined experimentally for a powder sample. Finally, we found the interactions between the individual layers of the molecules in the crystal, which have rather uniform effect on all ^{13}C NMR CSTs in the system (deshielding both in-plane components and shielding the out-of-plane component). Generally, the stacking interactions between aromatic systems are modulated by disperse forces. However, the ^{13}C NMR CSTs of individual atoms in these

aromatic systems are influenced simply by the interaction between two atoms of the neighboring layers resulting in the redistribution of electron density and its recoding into the magnetic shielding. Our concept can be used to investigate and interpret the modulations of the NMR observables by individual intermolecular and interfragment interactions in a range of systems, for example, stacking in biological macromolecules, particularly nucleic acids.

■ ASSOCIATED CONTENT

S Supporting Information

DFT calculated principal components of the ^{13}C CSTs for the largest supramolecular cluster obtained by using different geometries and density functionals; experimental principal components of the ^{13}C CSTs determined at different MAS frequencies; DFT calculated principal components of the ^{13}C CSTs for the two molecules in the asymmetric unit of the theobromine crystal structure embedded in the cluster **HB10**; visualization of the EDD and SDD for a stacked pair of molecules featuring an interaction which influences the CST of carbons C5 and C6; Cartesian coordinates of the supramolecular clusters. This information is available free of charge via the Internet at <http://pubs.acs.org>.

■ AUTHOR INFORMATION

Corresponding Author

*E-mail: rmarek@chemi.muni.cz.

Author Contributions

The manuscript was written through contributions of all authors. All authors have given approval to the final version of the manuscript.

Notes

The authors declare no competing financial interest.

■ ACKNOWLEDGMENTS

The authors thank the Czech Science Foundation for financial support (Grant No. P206/11/0550). Access to the computing and storage facilities owned by parties and projects contributing to the National Grid Infrastructure MetaCentrum provided under the program “Projects of Large Infrastructure for Research, Development, and Innovations” (LM2010005) and the CERIT-SC computing and storage facilities provided under the program Center CERIT Scientific Cloud, part of the Operational Program Research and Development for Innovations, Reg. No. CZ. 1.05/3.2.00/08.0144 is highly appreciated.

■ ABBREVIATIONS

NMR, nuclear magnetic resonance; DFT, density functional theory; CST, chemical shift tensor; EDD, electron deformation density; SDD, shielding deformation density; HB, hydrogen bonding; S, $\pi \cdots \pi$ stacking; HBS, hydrogen-bonding and $\pi \cdots \pi$ stacking

■ REFERENCES

- (1) Braga, D.; Grepioni, F.; Maini, L.; Polito, M. Crystal Polymorphism and Multiple Crystal Forms. In *Molecular Networks*; Hosseini, M. W., Ed.; Springer-Verlag: Berlin Heidelberg, Germany, 2009; Vol. 132, pp 25–50.
- (2) Brittain, H. G. *J. Pharm. Sci.* **2010**, 99, 3648–3664.
- (3) Lu, J.; Rohani, S. *Curr. Med. Chem.* **2009**, 16, 884–905.
- (4) Burrows, A. D. Crystal Engineering Using Multiple Hydrogen Bonds. In *Supramolecular Assembly via Hydrogen Bonds I*; Mingos, D.

- M. P., Ed.; Springer-Verlag: Berlin Heidelberg, Germany, 2004; Vol. 108, pp 55–96.
- (5) Harris, R. K. *Analyst* **2006**, *131*, 351–373.
- (6) Sergeyev, I. V.; Day, L. A.; Goldbourt, A.; McDermott, A. E. *J. Am. Chem. Soc.* **2011**, *133*, 20208–20217.
- (7) Potrzebowksi, M. J. *Organic and Pharmaceutical Chemistry*. In *NMR Crystallography*; Harris, R. K., Wasylshen, R. E., Duer, M. J., Eds.; John Wiley and Sons, Ltd.: Chichester, West-Sussex, United Kingdom, 2009; pp 435–453.
- (8) Facelli, J. C. *Prog. NMR Spectrosc.* **2011**, *58*, 176–201.
- (9) Ma, Z.; Halling, M. D.; Solum, M. S.; Harper, J. K.; Orendt, A. M.; Facelli, J. C.; Pugmire, R. J.; Grant, D. M.; Amick, A. W.; Scott, L. T. *J. Phys. Chem. A* **2007**, *111*, 2020–2027.
- (10) Maliňáková, K.; Novosadová, L.; Pipíška, M.; Marek, R. *ChemPhysChem* **2011**, *12*, 379–388.
- (11) Case, D. A. NMR Parameters in Proteins and Nucleic Acids. In *Calculation of NMR and EPR Parameters. Theory and Applications*; Kaupp, M., Bühl, M., Malkin, V., Eds.; WILEY-VCH Verlag GmbH & Co. KGaA: Weinheim, Germany, 2004; pp 341–351.
- (12) Wilson, P. J. *Annu. Rep. NMR Spectrosc.* **2003**, *49*, 117–168.
- (13) Di Fiori, N.; Orendt, A. M.; Caputo, M. C.; Ferraro, M. B.; Facelli, J. C. *Magn. Reson. Chem.* **2004**, *42*, S41–S47.
- (14) Malkin, V. G.; Malkina, O. L.; Salahub, D. R. *J. Am. Chem. Soc.* **1995**, *117*, 3294–3295.
- (15) Facelli, J. C.; Pugmire, R. J.; Grant, D. M. *J. Am. Chem. Soc.* **1996**, *118*, 5488–5489.
- (16) Pickard, C. J.; Mauri, F. *Phys. Rev. B* **2001**, *63*, 245101–245113.
- (17) Babinský, M.; Bouzková, K.; Pipíška, M.; Novosadová, L.; Marek, R. *J. Phys. Chem. A* **2013**, *117*, 497–503.
- (18) Scheiner, S.; Kar, T. *J. Phys. Chem. A* **2002**, *106*, 1784–1789.
- (19) Kolman, V.; Babinský, M.; Kulhánek, P.; Marek, R.; Šindelář, V. *New J. Chem.* **2011**, *35*, 2854–2859.
- (20) Maliňáková, K.; Novosadová, L.; Lahtinen, M.; Kolehmainen, E.; Brus, J.; Marek, R. *J. Phys. Chem. A* **2010**, *114*, 1985–1995.
- (21) Ford, K. A.; Ebisuzaki, Y.; Boyle, P. D. *Acta Cryst. C* **1998**, *C54*, 1980–1983.
- (22) Opella, S. J.; Frey, M. H. *J. Am. Chem. Soc.* **1979**, *101*, 5854–5856.
- (23) Xiaoling, W.; Shanmin, Z.; Xuewen, W. *J. Magn. Reson.* **1988**, *77*, 343–347.
- (24) Massiot, D.; Fayon, F.; Capron, M.; King, I.; Le Calvé, S.; Alonso, B.; Durand, J.-O.; Bujoli, B.; Gan, Z.; Hoatson, G. *Magn. Reson. Chem.* **2002**, *40*, 70–76.
- (25) Antzutkin, O. N. *Prog. Nucl. Magn. Reson. Spectrosc.* **1999**, *35*, 203–266.
- (26) Mason, J. *Solid State Nucl. Magn. Reson.* **1993**, *2*, 285–288.
- (27) Frisch, M. J.; Trucks, G. W.; Schlegel, H. B.; Scuseria, G. E.; Robb, M. A.; Cheeseman, J. R.; Scalmani, G.; Barone, V.; Mennucci, B.; Petersson, G. A.; Nakatsuji, H.; Caricato, M.; Li, X.; Hratchian, H. P.; Izmaylov, A. F.; Bloino, J.; Zheng, G.; Sonnenberg, J. L.; Hada, M.; Ehara, M.; Toyota, K.; Fukuda, R.; Hasegawa, J.; Ishida, M.; Nakajima, T.; Honda, Y.; Kitao, O.; Nakai, H.; Vreven, T.; Montgomery, Jr., J. A.; Peralta, J. E.; Ogliaro, F.; Bearpark, M.; Heyd, J. J.; Brothers, E.; Kudin, K. N.; Staroverov, V. N.; Kobayashi, R.; Normand, J.; Raghavachari, K.; Rendell, A.; Burant, J. C.; Iyengar, S. S.; Tomasi, J.; Cossi, M.; Rega, N.; Millam, J. M.; Klene, M.; Knox, J. E.; Cross, J. B.; Bakken, V.; Adamo, C.; Jaramillo, J.; Gomperts, R.; Stratmann, R. E.; Yazyev, O.; Austin, A. J.; Cammi, R.; Pomelli, C.; Ochterski, J. W.; Martin, R. L.; Morokuma, K.; Zakrzewski, V. G.; Voth, G. A.; Salvador, P.; Dannenberg, J. J.; Dapprich, S.; Daniels, A. D.; Farkas, Ö.; Foresman, J. B.; Ortiz, J. V.; Cioslowski, J.; Fox, D. J. *Gaussian 09*, Revision A.2; Gaussian, Inc.: Wallingford, CT, 2009.
- (28) Becke, A. D. *Phys. Rev. A* **1988**, *38*, 3098–3100.
- (29) Becke, A. D. *J. Chem. Phys.* **1993**, *98*, 5648–5652.
- (30) Stephens, P. J.; Devlin, F. J.; Chabalowski, C. F.; Frisch, M. J. *J. Phys. Chem.* **1994**, *98*, 11623–11627.
- (31) McLean, A. D.; Chandler, G. S. *J. Chem. Phys.* **1980**, *72*, 5639–5648.
- (32) Zhao, Y.; Truhlar, D. G. *Theor. Chem. Acc.* **2008**, *120*, 215–241.
- (33) Krishnan, R.; Binkley, J. S.; Seeger, R.; Pople, J. A. *J. Chem. Phys.* **1980**, *72*, 650–654.
- (34) Adamo, C.; Barone, V. *J. Chem. Phys.* **1999**, *110*, 6158–6170.
- (35) Boys, S.; Bernardi, F. *Mol. Phys.* **1970**, *19*, 553–566.
- (36) TURBOMOLE V6.3.1; TURBOMOLE GmbH: Karlsruhe, Germany, 2011.
- (37) Grimme, S. *J. Chem. Phys.* **2003**, *118*, 9095–9102.
- (38) Dunning, T. *J. Chem. Phys.* **1989**, *90*, 1007–1023.
- (39) Kendall, R.; Dunning, T.; Harrison, R. *J. Chem. Phys.* **1992**, *96*, 6796–6806.
- (40) Weigend, F.; Häser, M. *Theor. Chem. Acc.* **1997**, *97*, 331–340.
- (41) Mauri, F.; Pfrommer, B. G.; Louie, S. G. *Phys. Rev. Lett.* **1996**, *77*, 5300–5303.
- (42) Yates, J. R.; Pham, T. N.; Pickard, C. J.; Mauri, F.; Amado, A. M.; Gil, A. M.; Brown, S. P. *J. Am. Chem. Soc.* **2005**, *127*, 10216–10220.
- (43) Schmidt, J.; Hoffmann, A.; Spiess, H. W.; Sebastiani, D. *J. Phys. Chem. B* **2006**, *110*, 23204–23210.
- (44) Webber, A. L.; Emsley, L.; Claramunt, R. M.; Brown, S. P. *J. Phys. Chem. A* **2010**, *114*, 10435–10442.
- (45) Klod, S.; Kleinpeter, E. *J. Chem. Soc., Perkin Trans. 2* **2001**, 1893–1898.
- (46) Klod, S.; Koch, A.; Kleinpeter, E. *J. Chem. Soc., Perkin Trans. 2* **2002**, 1506–1509.